Scheme 1. Nitroxyl Radical Reduction and Oxidation Sensors

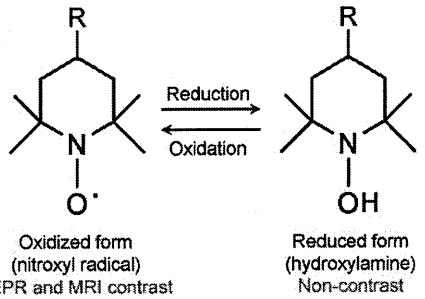

could be reconverted via oxygenation to paramagnetic nitroxyl radical with an appearance of EPR or ^{1}H-MRI relaxivity and thus serve as an oxidation sensor. The rate constants of both processes could be used for evaluation of reduction/oxidation balance in cells and tissues, using EPR imaging (EPRI) or MRI (Scheme 1).

Some nitroxyl radicals can easily gain an excellent cell permeability and even a permeability for blood−brain barrier (BBB) by simple chemical modification.[11−15] All these characteristics make them attractive for MRI diagnostics, and their application in life science research could be extended beyond the limits, mentioned above. In this context, we supposed that the nitroxyl radicals could be appropriate spin-labels of conventional therapeutics: for noninvasive MR imaging of their permeability for BBB and their localization in different organs and tissues. Most EPR studies, targeting the brain, have employed pyrrolidine-type (PROXYL-type) nitroxyl radicals, which have a higher stability *in vivo* in comparison with piperidine-type (TEMPO-type) nitroxyl radicals due to the low temporal resolution of CW-based techniques.[12−15] The higher temporal resolution of MRI allows an observation of pharmacokinetics of piperidine-type nitroxyl radicals.[9,16] In addition, MRI is characterized by much higher spatial resolution than EPRI and gives an excellent anatomical reference, which could facilitate the exact localization of a nitroxyl-labeled drug in the organism. Below, we would like to describe the impact of this approach and to give a proof for the reality of this concept.

The noninvasive, real-time imaging of drug permeability for BBB and localization in different brain compartments (drug brain mapping) is an indispensible step in the preclinical and clinical testing of new therapeutics for brain diseases. The precise mapping of a drug in the target or nontarget tissue has a significant impact for its dosing and prognostication of its target-specific effect and side effects.

The conventional methods for investigation of BBB permeability are usually invasive and time- and cost-consuming, often suffering from artifacts, and requiring a large number of experimental animals.[17−22] *In vitro* models of BBB (e.g., cell and tissue cultures, immobilized artificial

(2) Keana, J. F.; Pou, S.; Rosen, G. M. Nitroxides as potential contrast enhancing agents for MRI application: influence of structure on the rate of reduction by rat hepatocytes, whole liver homogenate, subcellular fractions, and ascorbate. *Magn. Reson. Med.* **1987**, *5*, 525–536.

(3) Valgimigli, L.; Pedulli, G. F.; Paolini, M. Measurement of oxidative stress by EPR radical-probe technique. *Free Radical Biol. Med.* **2001**, *31*, 708–716.

(4) Utsumi, H.; Yamada, K. In vivo electron spin resonance-computed tomography/nitroxyl probe technique for non-invasive analysis of oxidative injuries. *Arch. Biochem. Biophys.* **2003**, *416*, 1–8.

(5) Takeshita, K.; Ozawa, T. Recent progress in in vivo ESR spectroscopy. *J. Radiat. Res. (Tokyo)* **2004**, *45*, 373–384.

(6) Soule, B. P.; Hyodo, F.; Matsumoto, K.; Simone, N. L.; Cook, J. A.; Krishna, M. C.; Mitchell, J. B. Therapeutic and clinical applications of nitroxide compounds. *Antioxid. Redox Signaling* **2007**, *9*, 1731–1743.

(7) Afzal, V.; Brasch, R. C.; Nitecki, D. E.; Wolff, S. Nitroxyl spin label contrast enhancers for magnetic resonance imaging. Studies of acute toxicity and mutagenesis. *Invest. Radiol.* **1984**, *19*, 549–552.

(8) Matsumoto, K.; Hyodo, F.; Matsumoto, A.; Koretsky, A. P.; Sowers, A. L.; Mitchell, J. B.; Krishna, M. C. High-resolution mapping of tumor redox status by MRI using nitroxides as redox-sensitive contrast agents. *Clin. Cancer Res.* **2006**, *12*, 2455–2462.

(9) Hyodo, F.; Matsumoto, K.; Matsumoto, A.; Mitchel, J. B.; Krishna, M. C. Probing the intracellular redox status of tumors with MRI and redox-sensitive contrast agents. *Cancer Res.* **2006**, *66*, 9921–9928.

(10) Hyodo, F.; Matsumoto, K.; Matsumoto, A.; Mitchel, J. B.; Krishna, M. C. Probing the intracellular redox status of tumors with MRI and redox-sensitive contrast agents. *Cancer Res.* **2006**, *66*, 9921–9928.

(11) Hyodo, F.; Chuang, K.-H.; Goloshevsky, A. G.; Sulima, A.; Griffiths, G. L.; Mitchell, J. B.; Koretsky, A. P.; Krishna, M. C. Brain redox imaging using blood-brain barrier-permeable nitroxide MRI contrast agent. *J. Cereb. Blood Flow Metab.* **2008**, 1–10.

(12) Myiake, M.; Shen, J.; Liu, S.; Shi, H.; Liu, W.; Yuan, Z.; Pritchard, A.; Kao, J. P. Y.; Liu, K. J.; Rosen, G. M. Acetoxymethoxycarbonyl nitroxides as EPR proimaging agents to measure O2 levels in mouse brain: A pharmacokinetic and pharmacodynamic study. *J. Pharmacol. Exp. Ther.* **2006**, *318*, 1187–1193.

(13) Shen, J.; Liu, S.; Miyake, M.; Liu, W.; Pritchard, A.; Kao, J. P. Y.; Rosen, G. M.; Tong, Y.; Liu, K. J. Use of 3-acetoxymethoxy-carbonyl-2,2,5,5-tetramethyl-1-pyrrolidinyloxyl as an EPR oximetry probe: Potential for in vivo measurement of tissue oxygenation in mouse brain. *Magn. Reson. Med.* **2006**, *55*, 1433–1440.

(14) Sano, H.; Naruse, M.; Matsumoto, K.; Oi, T.; Utsumi, H. A new nitroyxl-probe with high retention in the brain and its application for brain imaging. *Free Radical Biol. Med.* **2000**, *28*, 959–969.

(15) Anzai, K.; Saito, K.; Takeshita, K.; Takahashi, S.; Miyazaki, H.; Shoji, H.; Lee, M. C.; Masumizu, T.; Ozawa, T. Assessment of ESR-CT imaging by comparison with autoradiography for the distribution of a blood-brain-barrier permeable spin probe, MC-PROXYL, to rodent brain. *Magn. Reson. Imaging* **2003**, *21*, 765–772.

(16) Cotrim, A. P.; Hyodo, F.; Matsumoto, K.; Sowers, A. L.; Cook, J. A.; Baum, B. J.; Krishna, M. C.; Mitchell, J. B. Differential radiation protection of salivary glands versus tumor by tempol with accompanying tissue assessment of tempol by magnetic resonance imaging. *Clin. Cancer Res.* **2007**, *13*, 4928–4933.

(17) Zhang, L.; Zhu, H.; Oprea, T. I.; Golbraikh, A.; Tropsha, A. QSAR modeling of the blood-brain barrier permeability for diverse organic compounds. *Pharm. Res.* **2008**, *25*, 1902–1914.

(18) Shen, D. D.; Artru, A. A.; Adkison, K. K. Principles and applicability of CSF sampling for the assessment of CNS drug delivery and pharmacodynamics. *Adv. Drug Delivery Rev.* **2004**, *56*, 1825–1857.

membranes, etc.) often serve as a major approach for indirect evaluation of drug delivery in the brain tissue. The development of new methodologies for *in vivo* imaging of BBB permeability, which are noninvasive, environmentally friendly, with minimal animal loss and minimal risk for volunteers, is a major goal of the modern pharmaceutical industry.

Currently, the radiopharmaceuticals combined with autoradiography or positron-emission tomography (PET) are the only option for noninvasive real-time imaging of BBB permeability.[23−25] Despite that this approach is highly sensitive and valuable, it suffers from several restrictions to be widely applicable in preclinical and clinical testing of new therapeutics. The radiolabeling possesses a risk for human safety and requires special experimental equipment and facilities, which increases markedly the cost of this analysis. The radiotracers are usually used for labeling of diagnostic markers, but not for labeling of therapeutics and noninvasive imaging of their permeability and localization in different organs.

In the present study, we would like to introduce a novel nonradioactive and environmentally friendly alternative for noninvasive real-time imaging of BBB permeability for conventional drugs, using stable nitroxyl radicals as spin-labels and MRI. To clarify the advisability of this approach, we have to prove that (i) the nitroxyl-labeled drug is stable in physiological fluids and there is no dissociation of nitroxyl-drug bond in the blood; and (ii) the nitroxyl-labeling does not affect significantly the drug pharmacodynamics, its toxicity and permeability for BBB.

We considered the anticancer drug lomustine [1-(2-chloroethyl)-3-cyclohexyl-1-nitrosourea, CCNU] as an appropriate model for spin-labeling and nitroxyl radical TEMPO as an appropriate spin-label for this particular case. Lomustine has a significant impact in the improvement of the health-related quality of life of patients, treated for brain tumors, as well as of any other patients with cancer.[26] Both substances (TEMPO-radical and lomustine) are permeable for BBB,[16,27] and the TEMPO radical has a 6-membered ringed structure as the cyclohexyl part of lomustine molecule.

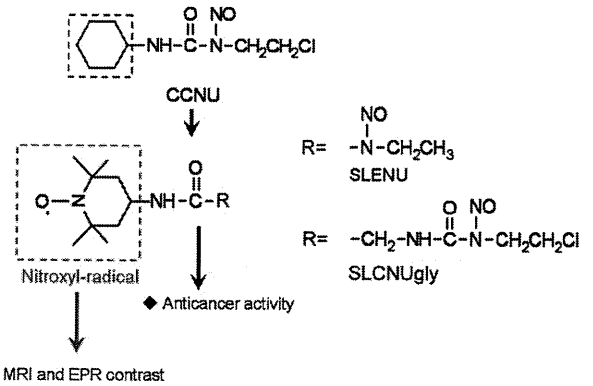

Figure 1. (A) Lomustine (CCNU) and its nitroxyl-labeled analogues (SLENU and SLCNUgly).

The lomustine molecule could be formally separated into two parts (Figure 1). The nitrosourea ensures the anticancer effect and could not be modified. Thus, the cyclohexyl part of lomustine was exchanged with TEMPO radical. We supposed that this substitution keeps a low risk for influence of drug pharmacodynamics in the organism, its toxicity and anticancer effect.

Two TEMPO-labeled analogues (SLENU and SLCNUgly) of lomustine (originally synthesized) (Figure 1) and one commercial nitroxyl (TEMPOL) were used in EPR and MRI experiments. All substances were characterized with different hydrophobicity [classified as slightly hydrophobic (TEMPOL), hydrophobic (SLENU), and strongly hydrophobic (SLCNUgly)], cell permeabilization ability and blood clearance. Thus, it was possible to investigate the relationship between the structure of nitroxyl-labeled drug, its half-life in the circulation, its permeability for BBB and MRI signal dynamic in the brain. This information was important for estimation of the merits and demerits of the described approach and finding pathways for overcoming the restrictions.

Experimental Methods

Chemicals. TEMPOL (4-hydroxy-2,2,6,6-tetramethyl-1-piperidin-1-oxyl) was purchased from Sigma-Aldrich.

Nitroxyl-labeled nitrosoureas SLENU {1-ethyl-3-[4-(2,2,6,6-tetramethylpiperidine-1-oxyl)]-1-nitrosourea} and SLCNUgly {1-chloroethyl-3-[4-glycine-(2,2,6,6-tetrameth-

(19) Pan, D.; Iyer, M.; Liu, J.; Li, Y.; Hopfinger, A. J. Constructing optimum blood brain barrier QSAR models using a combination of 4D-molecular similarity measures and cluster analysis. *J. Chem. Inf. Comput. Sci.* **2004**, *44*, 2083–2098.
(20) Dash, A. K.; Elmquist, W. F. Separation methods that are capable of revealing blood-brain barrier permeability. *J. Chromatogr., B: Anal. Technol. Biomed. Life Sci.* **2003**, *797*, 241–254.
(21) Gumbleton, M.; Audus, K. L. Progress and limitations in the use of in vitro cell cultures to serve as a permeability screen for the blood-brain barrier. *J. Pharm. Sci.* **2001**, *90*, 1681–1698.
(22) Killian, D. M.; Gharat, L.; Chikhale, P. J. Modulating blood-brain barrier interactions of amino acid-based anticancer agents. *Drug Delivery* **2000**, *7*, 21–25.
(23) Josserand, V.; Pélerin, H.; de Bruin, B.; Jego, B.; Kuhnast, B.; Hinnen, F.; Ducongé, F.; Boisgard, R.; Beuvon, F.; Chassoux, F.; Daumas-Duport, C.; Ezan, E.; Dollé, F.; Mabondzo, A.; Tavitian, B. Evaluation of drug penetration into the brain: a double study by in vivo imaging with positron emission tomography and using an in vitro model of the human blood-brain barrier. *J. Pharmacol. Exp. Ther.* **2006**, *316*, 79–86.
(24) Abbott, N. J.; Chugani, D. C.; Zaharchuk, G.; Rosen, B. R.; Lo, E. H. Delivery of imaging agents into brain. *Adv. Drug Delivery Rev.* **1999**, *37*, 253–277.
(25) Weissleder, R.; Mahmood, U. Molecular imaging. *Radiology* **2001**, *219*, 316–333.
(26) Taphoorn, M. J. B.; Van den Bent, M. J.; Mauer, M. E. L.; Coens, C.; Delattre, J.-Y.; Brandes, A. A.; Smitt, P. A. E.; Besrnsen, H. J. J. A.; Frenay, M.; Tijssen, C. C.; Lacombe, D.; Allgeier, A.; Bottomley, A. Health-related quality of life in patients treated for anaplastic oligodendroma with adjuvant chemotherapy: Results of a European Organisation for Research and Treatment of Cancer Randomized Clinical Trial. *J. Clin. Oncol.* **2007**, *25*, 5723–5730.
(27) Bodor, N.; Buchwald, P. Recent advances in the brain targeting of neuropharmaceuticals by chemical delivery systems. *Adv. Drug Delivery Rev.* **1999**, *36*, 229–254.

ylpiperidine-1-oxyl)]-1-nitrosourea} were synthesized and purified according to Gadjeva et al.[28,29] (with slight modifications).

Deionized water (deionization by the Milli-Q system) was used for all experiments. Other chemicals used were of analytical or HPLC grade.

***In Vitro* EPR measurements.** SLENU, SLCNUgly, and TEMPOL were first dissolved in DMSO to prepare 200 mM stock solutions. These 200 mM solutions were diluted with PBS, containing 1% bovine serum albumin to prepare 2 mM standard solutions. Each solution was put into a glass capillary, and their X-band EPR spectra were measured on X-band EPR instrument (JEOL, Akishima, Japan) with a TE-mode cavity. The capillary tube was positioned in the center of the TE-mode cavity using a special sample holder. The measurements were made under the following conditions: microwave frequency = 9.4 GHz, magnetic field strength = 336 mT, microwave power = 2.0 mW, field modulation frequency = 100 kHz, field modulation amplitude = 0.063 mT, time constant = 0.01 s, sweep width = 10 mT, scan time (sweep time) = 1 min.

In parallel, 2 μL of 200 mM stock solutions of SLENU, SLCNUgly, or TEMPOL (in DMSO) were added to 198 μL freshly isolated blood (with heparin) and the EPR measurements were provided at the parameters mentioned above within 30 min scan time.

The rotational correlation time (τ_c) of nitroxyl derivatives in PBS and blood was calculated by the following equation (Figure 2):[30]

$$\tau_c = A\{R(-1) + R(+1) - 2\}\cdot\Delta H(0) \qquad (1)$$

$R(-1) = [I(0)/I(-1)]^{1/2}$, where $I(0)$ and $I(-1)$ are the amplitudes of line 2 and line 3 in the EPR spectrum, respectively; $R(+1) = [I(0)/I(+1)]^{1/2}$, where $I(0)$ and $I(+1)$ are the amplitudes of line 2 and line 1 in the EPR spectrum, respectively; $\Delta H(0)$ is a line 2 width; $A = 6.6 \times 10^{-10}$ s is a constant, calculated for TEMPO radical.

All calculations were made from the EPR spectra of the nitroxyl derivatives (2 mM) in PBS or freashly isolated blood from mouse (after 5 min incubation). In the text, the data are presented as mean values from three independent experiments (SD did not exceed 5%). The obtained values are approximated, since we used an *A*-value for TEMPO in all calculations.

The total nitroxyl concentration in the brain tissue was analyzed according to Hyodo et al.[10] In brief, the brain was isolated 10 min after the iv injection of nitroxyl derivative in the mouse (0.4 mmol/kg bw). The isolated brain was

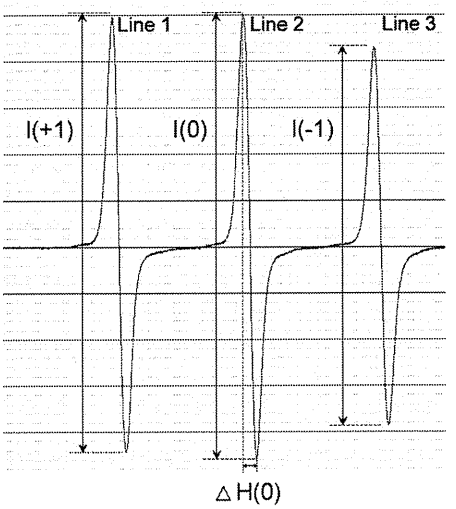

Figure 2. X-band EPR spectrum of TEMPO radical in PBS (pH 7.4) and characteristics used in the calculation of the rotational correlation time (τ_c).

rinsed several times by cold PBS, and the tissue (in equal weight for each animal) was homogenized in cold PBS. Ferricyanide (200 μL of 10 mM solution) was added to each homogenate (800 μL) to convert the reduced nitroxyl derivatives to their oxidized forms. EPR signal intensity was measured in tissue homogenates under the following conditions: modulation frequency, 100 kHz; microwave power, 1 mW. Finally, the concentration of nitroxyl derivative in the brain tissue was calculated based on a dilution factor of 5.

***In Vivo* EPR measurements.** The pharmacokinetic profiles of nitroxyl derivatives in mouse blood were measured using the method reported by Matsumoto et al.[31] C57Bl/6 mice (6 to 8 weeks of age at the time of experiments; mean weight ~25 g) were used. All experiments were conducted in accordance with the guidelines of the Physiological Society of Japan and were approved by the Animal Care and Use Committee of the National Institute of Radiological Sciences, Chiba, Japan.

The experimental design is shown in Scheme 2.

The mouse (~25 g) was anesthetized with 1.5% isoflurane using a face mask. The body temperature was kept within 36 ± 1 °C. The tail and jugular veins were cannulated by polyethylene tubing (PE10, Intramedic, Becton Dickinson Co.). The PE10 tubing from the jugular vein was placed in the TE-mode cavity of EPR instrument (JEOL, Akishima, Japan). The end of the tubing was connected to the syringe. All tubing and syringes were heparinized. The nitroxyl derivative was injected intravenously through the tail vein (0.4 mmol/kg bw; the drugs were dissolved in DMSO), and immediately after the injection the blood (~100 μL) was drained from the blood stream through the jugular vein to

(28) Gadjeva, V. Structure-based design of nitrosoureas containing tyrosine derivatives as potential antimelanoma agents. *Eur. J. Med. Chem.* **2002**, *37*, 295–300.

(29) Zheleva, A.; Gadjeva, V. Spin labelled nitrosoureas and triazenes and their non-labelled clinically used analogues--a comparative study on their physicochemical properties and antimelanomic effects. *Int. J. Pharmacol.* **2001**, *212*, 257–266.

(30) Hayashi, H.; Iwasaki, T.; Onodera, Y.; Nagase, T.; Itabashi, O. *Tohoku Kogyo Gijitsu Shikenjo Houkoku* **1992**, *29*, 33.

(31) Matsumoto, K.; Krishna, M. C.; Mitchell, J. B. Novel pharmacokinetic measurement using electron paramagnetic resonance spectroscopy and simulation of in vivo decay of various nitroxyl spin probes in mouse blood. *J. Pharmacol. Exp. Ther.* **2004**, *310*, 1076–1083.

Scheme 2. Scheme of Imaging of EPR Signal Dynamic of Nitroxyl Radical in the Blood Stream of Mouse under Anesthesia

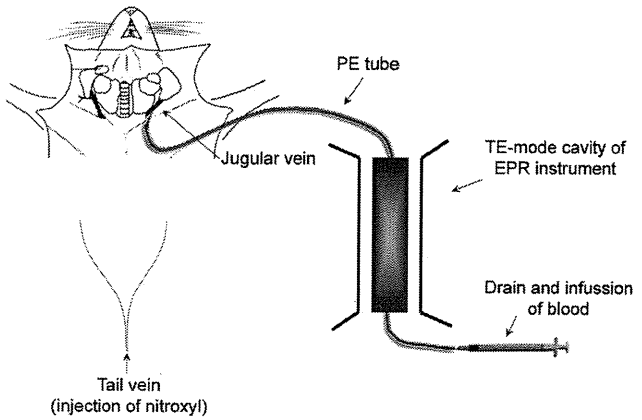

reach the TE-mode cavity of the EPR instrument. The EPR measurement was started. Immediately after finishing the measurement, the blood was infused back to the blood stream of the mouse. This cycle was repeated every 4−5 min within 30 min, to register the EPR signal dynamic of nitroxyl radical after its intravenous injection in the anesthetized animal. The EPR measurements were carried out in the same manner as described above.

***In Vivo* MRI Measurements.** MRI measurements were performed on a 7.0 T horizontal magnet (Kobelco and Jastec, Japan) interfaced to a Bruker Avance console (Bruker BioSpin, Germany) and controlled with ParaVision 4.0.1 (Bruker BioSpin, Germany).

The mouse (C57Bl/6, ~25 g) was anesthetized by isoflurane (1.2%) and placed in a head holder (Rapid Biomedical, Germany), stomach-side down and fixed head. A respiration sensor (SA Instruments, NY) was placed on the back of the mouse. A nonmagnetic temperature probe (FOT-M and FTI-10, FISO Technology, Germany) was used to monitor the rectal temperature of the mouse. The tail vein was cannulated by polyethylene tubing (PE10, Becton-Dickinson, NJ, USA) for injection of drug. The mouse was then placed in the ^{1}H-volume radiofrequency (RF) resonator (Brucker BioSpin) with surface RF receiver (Rapid Biomedical, Germany), which was previously warmed up using a body temperature controller (Rapid Biomedical). The resonator units, including the mouse, were placed in the magnet bore. The mouse body temperature was kept at 37 ± 1 °C during the MR measurements. Before the measurements after drug injection, five control images of the mouse brain were taken with the following parameters: T_1-weighted incoherent gradient-echo sequence (fast low-angle shot; FLASH), repetition time (TR) = 75 ms; echo time (TE) = 3.5 ms; flip angle (FA) = 45 degrees; field of view (FOV) = 3.2 × 3.2 cm; number of averages = 4; scan time = 19.6 s; matrix = 64 × 64; slice thickness = 1.0 mm; number of slices = 4. We selected coronal slice orientations with a 500 μm × 500 μm × 1000 μm nominal voxel resolution. One minute and 40 s after starting the scan, 100 μL of SLENU, SLCNUgly or TEMPOL (final dose, 0.4 mmol/kg bw; the drugs were dissolved in DMSO) was injected via the tail vein. T_1-weighted images were acquired continuously within ~20 min.

Mice, injected with DMSO only (in the same volume, 100 μL) served as controls.

The MRI data were analyzed using the ImageJ (National Institutes of Health, MD, USA) software.

All experiments were conducted in accordance with the guidelines of the Physiological Society of Japan and were approved by the Animal Care and Use Committee of the National Institute of Radiological Sciences, Chiba, Japan.

Results and Discussion

The substitution of the cyclohexyl part of the lomustine molecule with nitroxyl radical, as well as the substitution at the fourth position of the piperidine ring, did not affect significantly the toxicity and anticancer activity of nitrosourea. Using wild-type C57Bl/6 mice, we established the following LD50 values for nitroxyl derivatives: ~210 mg/kg bw for TEMPOL, ~100 mg/kg bw for SLENU, and ~125 mg/kg bw for SLCNUgly, versus ~56 mg/kg bw for lomustine (CCNU). The nitroxyl radical in SLENU and SLCNUgly decreased the toxicity of nitrosourea.

Using C57Bl/6 mice with experimental lymphoma L1210, we established the following optimal doses for anticancer activity of SLENU, SLCNUgly, and CCNU: ~45 mg/kg bw for SLENU and SLCNUgly, versus ~20 mg/kg for CCNU.

These preliminary data allowed the selection of the optimal dose for *in vivo* EPR and MR imaging of nitroxyl derivatives in C57Bl/6 mice. The doses, combining a comparatively low toxicity and comparatively high EPR and MRI contrast characteristics, were in the interval 0.2−0.4 mmol/kg bw, below the toxic limit or slightly close to the LD50 values of the described nitroxyl derivatives.

The first step of our study was to ensure that the TEMPO−nitrosourea bond is stable and there is no dissociation between both compounds in the blood. Thus, the detection of MRI signal enhancement of nitroxyl radical *in vivo* will indicate the localization of nitrosourea in the brain tissue.

In PBS, the normalized EPR spectra of TEMPOL, SLENU, and SLCNUgly were distinguished by the amplitude of the third line in the triplet [$I(-1)$] (Figure 3A). The lower amplitudes of line 3 in the EPR spectrum of SLENU and SLCNUgly could be explained by the limited motion of the nitrosourea-conjugated nitroxyl radical in comparison with free TEMPO radical (in the TEMPOL molecule). The larger the substitute at the fourth position of the piperidine ring, the slower the motion of the nitroxyl radical, which results in lower EPR signal enhancement. In PBS, the rotational correlations times (τ_c) of nitroxyl derivatives were 10.56 × 10^{-12} s, 29.45 × 10^{-12} s, and 31.38 × 10^{-12} s for TEMPOL, SLENU, and SLCNUgly, respectively.

In blood, the normalized EPR spectra had the same profiles as in PBS. There were no changes in the shape of the EPR spectra of SLENU and SLCNUgly during long-term incuba-

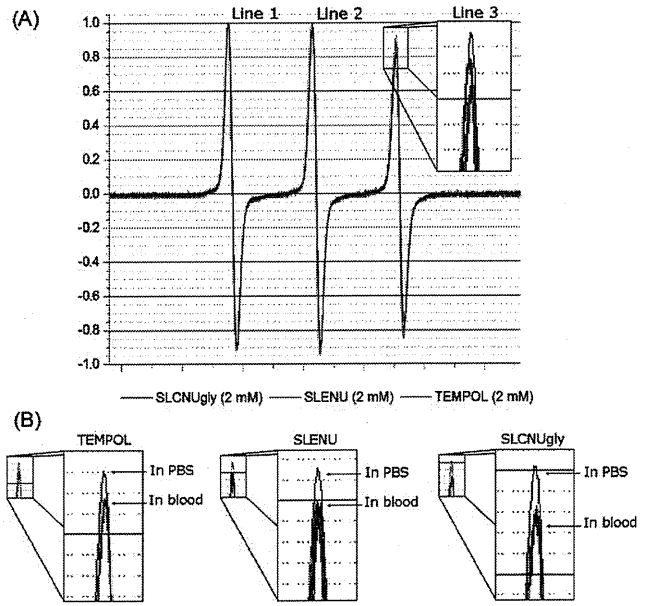

Figure 3. (A) Normalized EPR spectra of SLENU, SLCNUgly, and TEMPOL in PBS. In blood, the EPR spectra of all substances have same profiles. (B) Amplitudes of line 3 during long-term incubation of SLENU, SLCNUgly, and TEMPOL in freshly isolated blood samples *in vitro* (1−30 min). The amplitude of line 3 in PBS is shown for comparison.

tion in blood (Figure 3B), which indicated that there was no dissociation of the TEMPO−nitrosourea covalent bond. Only the amplitude of line 3 decreased in blood in comparison with PBS (Figure 3B). The rotational correlations times (τ_c) of nitroxyl derivatives in blood were 20.33×10^{-12} s, 32.87×10^{-12} s, and 46.20×10^{-12} s for TEMPOL, SLENU, and SLCNUgly, respectively. The data suggest that the motion of nitroxyl radical in blood decreased for each derivative, regardless of its hydrophobicity, presumably as a result of interaction between the drug and blood cells and/or lipoproteins.

In the second step, we investigated the blood clearance of nitroxyl derivatives *in vivo* in mice, using EPR spectroscopy (Scheme 2). This information allowed a prediction of the time necessary for transportation of nitroxyl derivative in the brain tissue (if it crosses BBB), which was important for design of the MRI measurements.

The kinetic curves of EPR signal dynamics of nitroxyl derivatives in the blood stream of living mice are shown in Figure 4. They were characterized with two phases: (i) an increase of the EPR signal within 1−1.5 min after the drug injection; and (ii) a decrease of the EPR signal within 1−5 min after the drug injection. The first phase is mainly a result of initial enhancement of the drug concentration in the blood stream. The second phase is probably a result of the following processes: (i) a reduction of nitroxyl radical in the blood plasma; and/or (ii) transportation of the drug from the blood stream to the blood cells and/or tissues and further reduction of nitroxyl radical from the cell/tissue reducing equivalents.

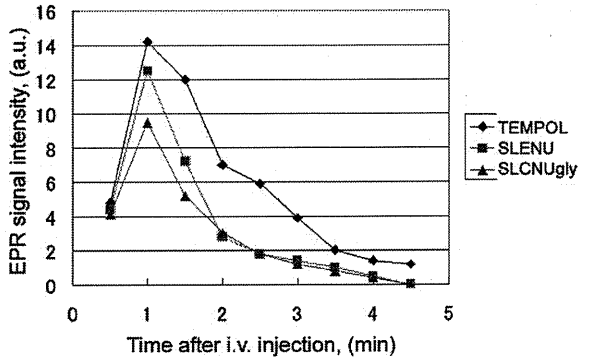

Figure 4. Dynamics of the EPR signal in the blood stream of mice under anesthesia after intravenous (iv) injection of nitroxyl derivative (0.4 mmol/kg bw). Mean values from three independent experiments are presented in the figure (SD values did not exceed 30%).

The time-decay of the EPR signal *in vivo* correlated with the hydrophobicity of nitroxyl derivative and its cell permeability. The rate of time-decay was slower for the low hydrophobic TEMPOL and faster for the hydrophobic SLENU and strongly hydrophobic SLCNUgly.

In vivo, the EPR signal of all nitroxyl derivatives disappeared rapidly in the blood (within 4−5 min after their injection). However, *in vitro* (in isolated blood samples), their EPR signal was comparatively stable within 1−30 min incubation (only ~5% decrease was detected within this time interval). Since all investigated nitroxyls were cell permeable, we may speculate that within 4−5 min the nitroxyl derivatives were delivered in the tissues.

In the third step of our study, the nitroxyl derivatives were injected intravenously in healthy mice via the tail vein and ^{1}H-MR imaging of the brain was performed on a 7.0 T horizontal MRI (Figure 5). The injected dose was 0.4 mmol/kg bw.

At the selected scanning parameters, the nitroxyl-radical manifested a good T_1 relaxivity and was detected in the brain (Figure 5). Other authors[8,9] have also demonstrated a good T_1 relaxivity of TEMPOL at similar concentrations on experimental phantoms and animals (mice) using 4.7 T MRI and high image resolution (128 × 128 or 256 × 256). Although nitroxyls have a lower relaxivity than conventional T_1 contrast agents such as gadolinium complexes, the volume distribution of nitroxyls is sufficiently greater because of better cell permeability,[35] and with improved sensitivity of

(32) Matsumoto, K.; Yakumaru, H.; Narazaki, M.; Nakagawa, H.; Anzai, K.; Ikehira, H.; Ikota, N. Modification of nitroxyl contrast agents with multiple spins and their proton T_1 relaxivity. *Magn. Reson. Imaging* **2008**, *26*, 117–121.

(33) Metz, J. M.; Smith, D.; Mick, R.; Lustig, R.; Mitchell, J.; Cherakuri, M.; Glatstein, E.; Hahn, S. M. A phase I study of topical Tempol for the prevention of alopecia induced by whole brain radiotherapy. *Clin. Cancer Res.* **2004**, *10*, 6411–6417.

(34) Ravizza, R.; Cereda, E.; Monti, E.; Gariboldi, M. B. The piperidine nitroxide Tempol potentiates the cytotoxic effects of Temozolomide in human glioblastoma cells. *Int. J. Oncol.* **2004**, *25*, 1817–1822.

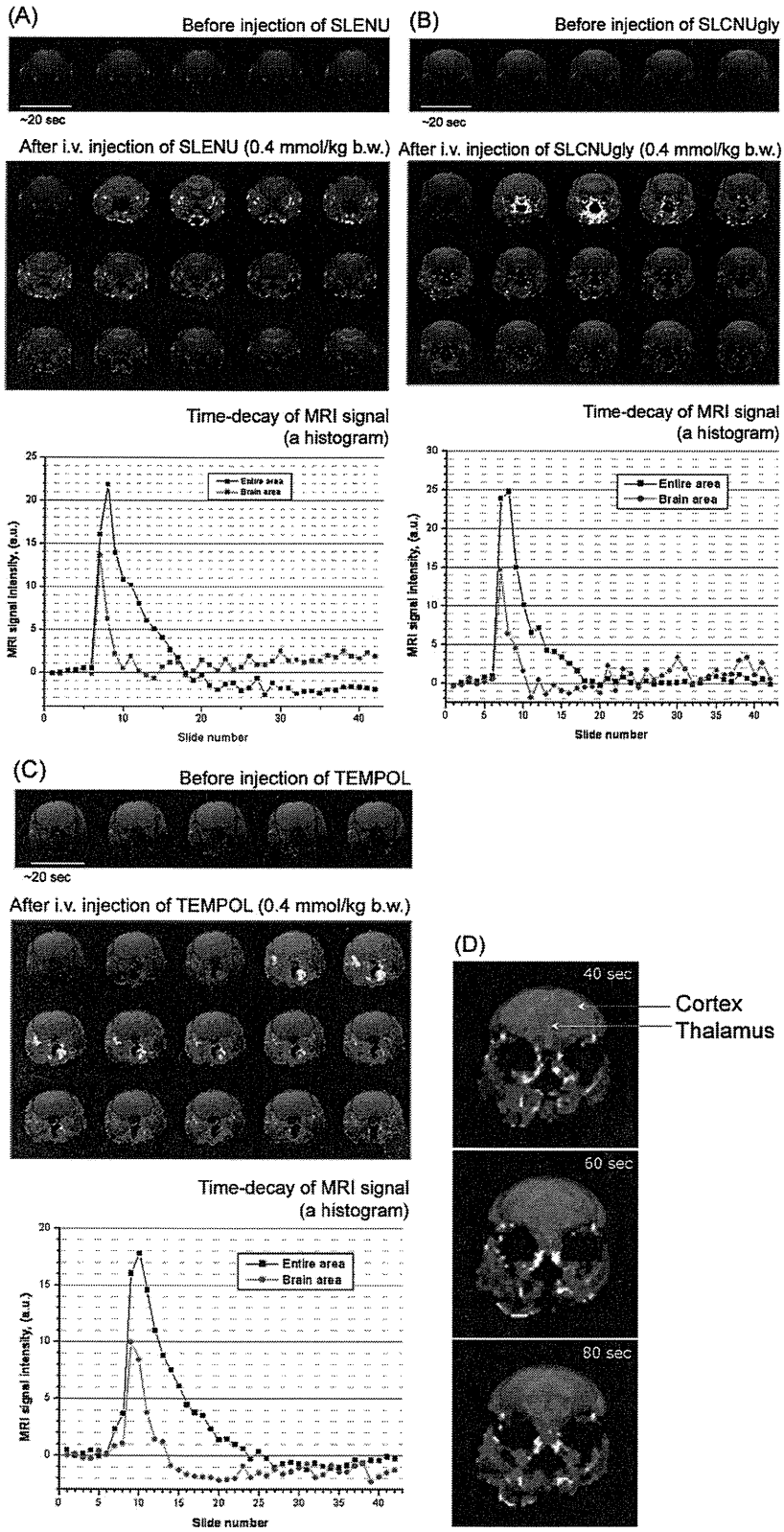

Figure 5. MRI signal dynamics of SLENU (A), SLCNUgly (B), and TEMPOL (C) in the brain and surrounding tissues after iv injection in mice (0.4 mmol/kg bw). Each image was obtained within a 20 s interval using a gradient-echo T_1-weighted MRI. The red color in the images is the extraction of the signal between every single slide and the averaged baseline signal (first 5 slides: before injection). The red and black colors in the chart represent MRI signal dynamics in the brain or entire area, respectively. A representative image from three independent experiments is shown in the figure. (D) MRI signal dynamics of SLENU in the brain compartments (cortex and thalamus) after its iv injection in mice (0.8 mmol/kg bw).

MRI and shift to higher magnetic fields, it is possible to detect nitroxyl radical in the tissues at low (nontoxic or low toxic) concentrations. In our study, using 7 T MRI and resolution 64 × 64, the MRI contrast of TEMPOL was high enough to detect the signal in the brain at concentrations 0.4 mmol/kg bw.

It is well-known that the nitrosoureas are highly permeable for cell membranes and BBB and are concentrated in the brain tissue. Therefore, it could be expected that the real concentration of SLENU and SLCNUgly in the brain tissue would be same as or even higher than the concentration of TEMPOL, and this should have a positive effect on MRI contrast of both nitroxyl-labeled drugs. We established that ~30% of the injected dose of SLENU and SLCNUgly was localized in the brain. The experiments were performed on tissue homogenates prepared from perfused brain, isolated 10 min after the iv injection of the drug.

The MRI-signal dynamics of SLENU and SLCNUgly (Figure 5A,B) in the brain and surrounding tissues followed almost the same kinetics and distribution as nonconjugated TEMPO radical (Figure 5C). The maximum change in the signal intensity (~25−30% in comparison with the preinjection image) in the brain tissue was detected 20, 20 or 80 s after the injection of SLENU, SLCNUgly, or TEMPOL, respectively. In the brain tissue, the MRI signal intensity decreased during the subsequent 2 min, while in the surrounding tissues, the MRI signal intensity decreased during the subsequent 4−5 min. Recently, Hyodo et al. have reported that the MRI signal of a BBB permeable nitroxyl, methoxycarbonyl-2,2,5,5-tetramethylpyrrolidine-1-oxyl, also disappeared quickly after its transportation from the blood vessels to the brain tissue, despite the slower reduction rate of pyrrolidine radical.[11]

SLENU and SLCNUgly were rapidly and randomly distributed into the brain tissue. For example, the nitroxyl derivatives were localized predominantly in the cortex and thalamus (Figure 5D). The MRI signal decay in the cortex was faster than the MRI signal decay in the thalamus. It may be speculated that the cortex has a higher reduction potential than the thalamus. Similar results were reported by Hyodo et al.[11]

Obviously, the exchange of the cyclohexyl part of lomustine with TEMPO radical did not suppress the permeability of the drug for the BBB. All investigated nitroxyl derivatives (TEMPOL, SLENU, SLCNUgly) manifested a similar permeability. This assumption was confirmed by using EPR spectroscopy for the assessment of the total concentration of nitroxyl derivative (converted to its oxidized form) in the brain tissue, isolated 10 min after the drug injection into mice. It was observed that the normalized EPR signal intensity of tissue homogenates, isolated from SLENU- and SLCNUgly-treated mice (2.3 ± 0.6 and 2.5 ± 0.4 a.u. per g of tissue, respectively), was slightly higher than the EPR signal intensity of homogenates, isolated from TEMPOL-treated mice (2.0 ± 0.5 a.u. per g of tissue). The data from diffusion-weighted MRI also confirmed that SLENU and SLCNUgly crossed the BBB. After free-water signal suppression by the diffusion-weighted MRI technique with motion probing gradients, the MRI signal remained in the brain tissue (data are not shown).

The MRI signal enhancement of nitroxyl radical disappeared quickly (within 2−3 min) after the transportation of SLENU and SLCNUgly from the brain vessels in the brain tissue. Presumably, this is due to the high permeability of nitroxyl-labeled nitrosoureas for cell membranes, which is accompanied with rapid reduction of nitroxyl radical to the respective hydroxylamine in the brain cells and loss of MRI signal enhancement. In the surrounding tissues, the MRI signal was more stable, with a bit longer half-life.

There was a good correlation between the rate of blood clearance of nitroxyl derivatives and their MRI signal dynamic in the brain and surrounding tissues. The faster the blood clearance of the drug (SLCNUgly = SLENU > TEMPOL), the faster the appearance of the MRI signal of the nitroxyl derivative in the brain and surrounding tissues (SLCNUgly = SLENU > TEMPOL) (Figures 4, 5).

The fast detection of MRI signal enhancement could be considered as an advantage, because of shortening of the time of analytical and diagnostic process.

The present data are just a first trial for using nitroxyl radicals for spin-labeling of conventional drugs and noninvasive dynamic MR imaging of their permeability for the BBB. We tried to show the advisability of this concept. Novel synthetic strategies are necessary to increase the contrast of nitroxyl label and to improve its stability in the brain tissue without affecting the drug permeability for BBB. This will allow a higher spatial resolution of signal-to-noise ratio and will facilitate the real-time MRI data reconstruction and quantitative analysis.

The enhancement of the MRI contrast of nitroxyl label is important for the wide application of the described methodology. This is a limiting factor, currently requiring the application of nitroxyl-labeled drug in a comparatively high concentration (0.2−0.4 mmol/kg bw), which sometimes could be near or over the toxic limit.

There are two promising strategies to increase the MRI contrast of nitroxyl label in the brain and other tissues: (i) the exchange of six-membered ringed nitroxyl TEMPO with five-membered ringed nitroxyl (2,2,5,5-tetramethyl-pyrrolidinyl-1-oxyl, PROXYL), which is characterized by higher relaxivity and ~10 times higher resistance to bioreduction than TEMPO radical;[2] and (ii) to develop new nitroxyl probes by modification of nitroxyl contrast agents with multiple spins (2 or more nitroxyl radicals bound covalently).

Matsumoto and colleagues have reported that a probe, consisting of three covalently bound PROXYL radicals, is characterized with 4-fold higher T_1 relaxivity than a single PROXYL radical. However, it is still unclear whether these multinitroxyl probes are permeable for BBB, cells and other tissues, to be applicable for labeling of conventional drugs

(35) Hahn, S. M.; Wilson, L.; Krishna, C. M.; Liebmann, J.; DeGraff, W.; Gamson, J.; Amuni, A.; Venzon, S.; Mitchell, J. Identification of nitroxide radioprotectors. *Radiat. Res.* **1992**, *123*, 87–93.

and noninvasive imaging of their localization in the organism. The low-molecular-weight cell- and BBB-permeable methoxycarbonyl-PROXYL seems promising for drug labeling and MR imaging in the brain. Recently, Hyodo and colleagues have used this nitroxyl derivative for evaluation of brain redox status by MRI. The MRI signal of methoxycarbonyl-PROXYL in the brain is comparatively high and stable within 4 min after the drug injection in mice. Our preliminary data also demonstrated that PROXYL is characterized with higher MRI contrast and slower MRI signal decay in the tissues (Figure 1S, Supporting Information). Currently, we are under way to clarify the applicability of PROXYL in the described methodology.

It is necessary also to note that nitroxyl radicals are low toxic and comparatively harmless for living organisms. One of the most famous commercially available nitroxyls, TEMPOL (hydroxyl-TEMPO), is in phase I of clinical trials, as a preventer of alopecia in radiation-treated cancer patients.[32] The combined application of nitroxyls and conventional chemotherapeutics increases the anticancer effect and suppresses the multidrug resistance.[33] Therefore, the nitroxyl-labeling could be considered as environmentally friendly and with minimal risk for humans. There is one more advantage in nitroxyl-labeling and imaging. The dynamic of MRI signal enhancement gives additional information for oxidation/reduction status of the brain tissue. This information could be useful for planning of conventional chemo- and radiotherapy of cancer and other diseases in the brain or other organs.

Acknowledgment. The technical support of Dr. Antoaneta Zheleva (Trakia University, Stara Zagora, Bulgaria) and Ms. Sayaka Shibata (Molecular Imaging Center, NIRS-Chiba, Japan) is gratefully acknowledged.

Supporting Information Available: Figure depicting the MRI signal dynamics of carbamoyl-PROXYL in the brain after iv injection in mice. This material is available free of charge via the Internet at http://pubs.acs.org.

MP800175K

J Neurosurg 111:28–36, 2009

Analysis of cerebral perfusion and metabolism assessed with positron emission tomography before and after carotid artery stenting

Clinical article

Shunji Matsubara, M.D., Ph.D.,[1] Junta Moroi, M.D., Ph.D.,[1] Akifumi Suzuki, M.D., Ph.D.,[1] Masahiro Sasaki, M.D., Ph.D.,[1] Ken Nagata, M.D., Ph.D.,[1] Iwao Kanno, Ph.D.,[2] and Shuichi Miura, Ph.D.[2]

Departments of [1]Strokology, and [2]Radiology and Nuclear Medicine, Research Institute for Brain and Blood Vessels–Akita, Akita, Japan

Object. The authors analyzed cerebral perfusion and metabolism in patients with internal carotid artery stenosis before and after carotid artery stenting (CAS).

Methods. Sixteen patients with internal carotid artery stenosis (> 70%) underwent PET scanning before CAS, 1–7 days after CAS, and 3–4 months after CAS to assess a variety of parameters related to cerebral perfusion and metabolism.

Results. Cerebral blood flow at rest (CBF_{rest}) significantly increased in the immediate postoperative stage before returning to normal levels over the long term; this trend was also recognized on the contralateral side. In contrast, there was gradual improvement in the rate of CBF variation on acetazolamide administration (% CBF_{az}). Cerebral perfusion pressure (CBF/cerebral blood volume) increased rapidly during the acute stage and decreased in the long term, and the oxygen extraction fraction decreased slightly during the acute stage before normalizing over the long term. The cerebral metabolic rate of oxygen ($CMRO_2$) increased slightly after stenting over both the short and long term. The ratios of ipsilateral to contralateral values (asymmetry index) for CBF_{rest}, % CBF_{az}, cerebral blood volume, oxygen extraction fraction, and $CMRO_2$ tended to approach 1.0 over time.

Conclusions. Repeated PET scanning revealed improvements in CBF, perfusion pressure, and oxygen metabolism after CAS. In particular, the vascular reserve tended to improve gradually, while CBF, cerebral perfusion pressure, and $CMRO_2$ increased rapidly and peaked soon after CAS. These results suggest that a large discrepancy between rapidly increased CBF, perfusion pressure, and a small increase in vascular reserve in the acute stage after CAS could cause hyperperfusion syndrome. *(DOI: 10.3171/2008.09.17663)*

Key Words • **carotid artery stenting** • **cerebral blood flow** • **hyperperfusion** • **PET** • **vascular reserve**

Internal CA stenosis sometimes causes cerebral ischemia either due to hemodynamic hypoperfusion or an artery-to-artery embolism. Although antiplatelet and/or anticoagulant pharmacotherapies are standard initial treatments for this disorder, CEA has been declared the gold standard not only for symptomatic ICA stenosis (≤ 70%),[26] but also for asymptomatic ICA stenosis (≤ 60%).[4]

Abbreviations used in this paper: CA = carotid artery; CAS = CA stenting; CBF = cerebral blood flow; CBF_{az} = CBF after acetazolamide challenge; CBF_{rest} = CBF at rest; CBV = cerebral blood volume; CEA = carotid endarterectomy; $CMRO_2$ = cerebral metabolic rate of oxygen; CPP = cerebral perfusion pressure; ICA = internal carotid artery; OEF = oxygen extraction fraction.

Carotid artery stenting was used in only a limited number of patients until several years ago because of the risk of intraoperative embolic cerebral ischemia. The recent development of protective devices has markedly improved treatment results,[9] and the current low rate of complications associated with CAS is mainly due to total protection systems such as PercuSurge GuardWire devices.[13,28] In addition, data from the Stenting and Angioplasty with Protection in Patients at High Risk for Endarterectomy Study[24] have demonstrated that CAS with an embolus protection device is not inferior to CEA in patients with severe CA stenosis and comorbidities. However, investigators in another recent multicenter trial of the use of

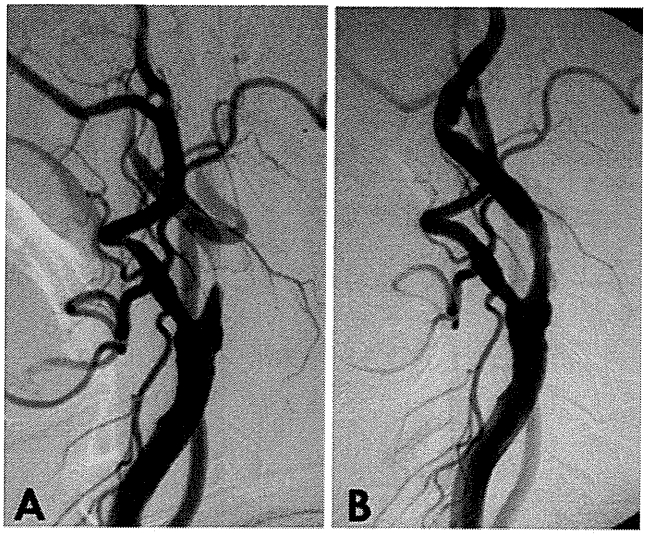

FIG. 1. Images obtained in the 71-year-old woman in the representative case. Preoperative right carotid injection angiogram confirming severe ICA stenosis (A). Right CA stenting was performed via the femoral artery without neurological sequelae. Postoperative angiography demonstrated no significant residual stenosis (B).

CAS with or without a protection device failed to prove safety compared to CEA.[36]

With respect to cerebral perfusion, analysis of SPECT data before and after CEA has revealed improvements in postoperative vasoreactivity,[2,15,16,34] but little is known about alterations in cerebral perfusion before and after CAS.[5,17,20] No previous studies have examined cerebral perfusion and metabolism on PET, with the exception of a small number of case reports describing distal ICA and basilar artery stenosis.[3,19,33] The present study is the first to describe alterations in cerebral perfusion and metabolism on PET scans obtained before and after CAS in patients with ICA stenosis.

Methods

Patient Population

Thirty-one patients with ICA stenosis ≥ 70% underwent CAS at our institution for a total of 34 lesions between April 2002 and March 2004. Positron emission tomography scanning was conducted before and after CAS in 28 lesions. Patients with coexisting conditions such as contralateral severe ICA stenosis or occlusion, or ipsilateral middle cerebral artery or distal ICA stenosis were excluded. Sixteen patients with 16 lesions participated in this study, including 12 men and 4 women with a mean age of 71.1 years (range 55–78 years) harboring 5 symptomatic and 11 asymptomatic lesions.

Protocol for CAS

A PercuSurge GuardWire system (Medtronic) was

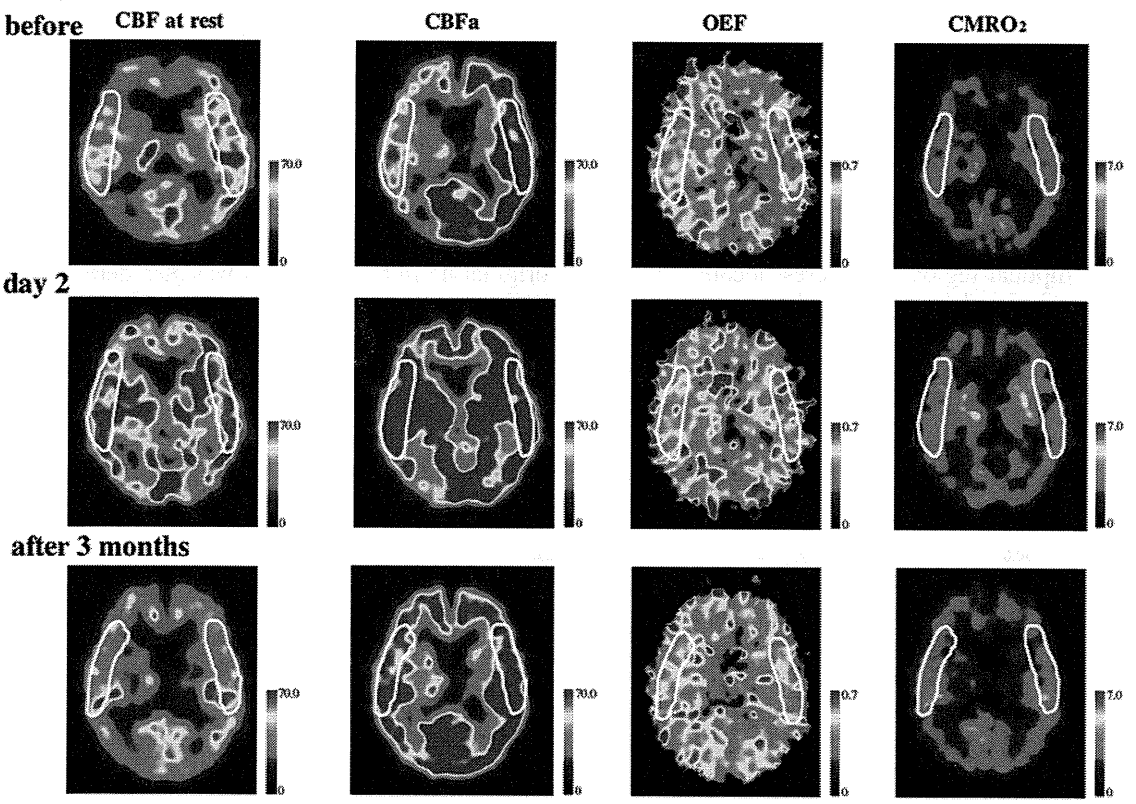

FIG. 2. Series of PET studies. *Upper Row:* Preoperative examinations detecting hypoperfusion and low vascular reserve in CBF_{rest} and CBF_{az}. No significant lateralities were noted in cerebral oxygen metabolism (OEF and $CMRO_2$). *Middle Row:* Studies obtained on postoperative Day 2 demonstrating a marked increase in CBF_{rest} and CBF_{az}, particularly on the affected side. The $CMRO_2$ increased subtly on the affected side. *Bottom Row:* Postoperative examination obtained 3 months after CAS confirming the absence of laterality for CBF_{rest} and improvements in CBF_{az}.

used as a distal ICA protection system in 15 patients, and a Naviballoon system (Kaneka) was used in 1 patient. With the patient under local anesthesia, a guiding catheter was advanced to the affected common CA, and a self-expandable SMART stent (Cordis Endovascular System) was implanted after predilation with a balloon catheter. Postdilation using a larger balloon catheter was used in 5 patients. For prevention of postoperative stroke related to stenting, 81 mg of aspirin and 200 mg of ticlopidine were routinely administered before CAS. Heparin was intravenously administered during and after CAS in all patients. No complications including cerebral ischemia, retinal ischemia, or groin hematoma occurred during peri- and postoperative stenting in any patient. Postoperative diffusion-weighted MR imaging was routinely performed, and no fresh infarctions that might affect the PET data were found in any patient.

Protocol for PET

Positron emission tomography was conducted 3 times: within 1 month before CAS, 1–7 days after CAS (acute stage), and 3–4 months after CAS. Only 8 patients underwent PET scanning 3–4 months postoperatively. A Headtome V (Shimazu) PET system was used to examine the following parameters: CBF_{rest}, OEF, and CBV using $^{15}O_2$-labeled water, $^{15}O_2$-labeled molecular O_2, or $^{15}O_2$-labeled CO, as previously reported.[18] The $CMRO_2$ and the CBF/CBV ratios were also calculated. The CBF/CBV ratio is an index of CPP according to the previous PET analysis of the relationship between CBF, CBV, and the oxygen extraction ratio.[8] Acetazolamide challenge was performed by intravenous administration of 1000 mg acetazolamide, and the percentage change in CBF from the resting state to the acetazolamide challenge state was calculated as follows: $\%\ CBF_{az} = 100 \times (CBF_{az} - CBF_{rest})/CBF_{rest}$.

Positron emission tomography analysis was performed using elliptical regions of interest located at the centrum semiovale level in each cerebral hemisphere.

TABLE 1: Mean values of the parameters before and after CAS

Parameter	Before	Acute Stage	Chronic Stage
ipsilateral side			
CBFrest (ml/100 ml/min)	37.6 ± 7.9	49.0 ± 10.1	39.1 ± 5.9
$\%CBF_{az}$ (%)	39.9 ± 21.5	42.8 ± 17.4	53.6 ± 13.0
CBV (ml/100g)	3.45 ± 0.69	3.48 ± 0.75	3.41 ± 0.53
CPP (min)	11.12 ± 2.26	14.25 ± 1.99	11.82 ± 3.22
OEF	0.44 ± 0.05	0.43 ± 0.06	0.45 ± 0.03
$CMRO_2$ (ml/100 ml/min)	2.62 ± 0.39	2.73 ± 0.37	2.71 ± 0.33
contralateral side			
CBF_{rest} (ml/100 ml/min)	40.5 ± 7.2	48.1 ± 10.1	39.7 ± 6.7
$\%CBF_{az}$ (%)	53.8 ± 15.7	45.5 ± 17.0	53.0 ± 16.1
CBV (ml/100g)	3.63 ± 0.72	3.66 ± 0.66	3.30 ± 0.46
CPP (min)	11.33 ± 1.86	13.34 ± 2.78	12.36 ± 3.14
OEF	0.42 ± 0.04	0.44 ± 0.06	0.44 ± 0.05
$CMRO_2$ (ml/100 ml/min)	2.75 ± 0.39	2.78 ± 0.38	2.69 ± 0.29

These data assessed from the affected side were compared with those for the control side at each stage. Values were statistically analyzed with unpaired t-tests using StatView 5.0 software (SAS Institute). Probability values < 0.05 were considered statistically significant.

Results

Representative Case

A 71-year-old woman developed pulse-synchronous tinnitus in her right ear. Significant coronary artery stenosis requiring bypass surgery was identified, but stenosis originating in the right ICA was also detected after cerebral angiography. The patient was referred to our institu-

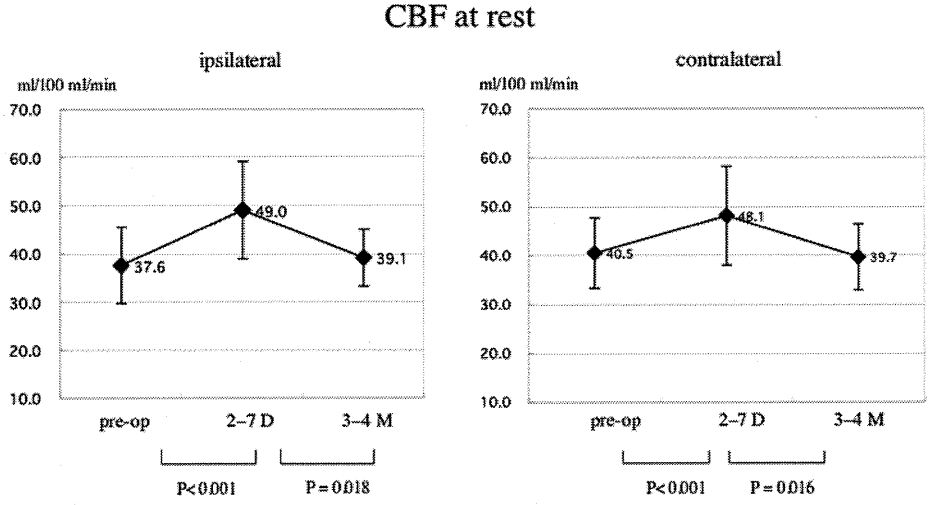

FIG. 3. Graphs showing sequential changes in CBF_{rest} on both sides. Ipsilaterally, significant increases are seen in the postoperative acute stage, with modest increases in the chronic stage. Contralaterally, significant increases are also seen in the acute stage, which reverted to the preoperative level in the chronic stage.

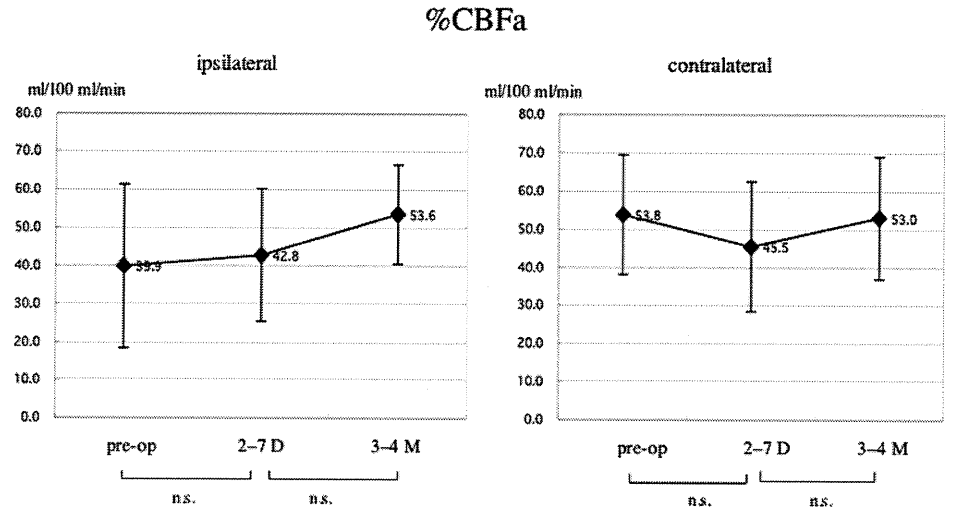

FIG. 4. Graphs showing sequential changes in % CBF_{az}. Mean values initially fell on the affected side but improved over time.

tion for CAS prior to coronary artery bypass. Initial right carotid injection angiography revealed 90% ICA stenosis (Fig. 1A). Angioplasty with a stent was successfully performed with the patient under local anesthesia, and no significant stenosis remained (Fig. 1B). Figure 2 depicts the PET scans and elliptical regions of interest used in this study.

Cerebral Blood Flow

As shown in Table 1, the ipsilateral CBF_{rest} significantly increased in the postoperative acute stage (by a median value of 30.3%) before returning to normal levels 3–4 months postoperatively. The contralateral side also exhibited this trend, increasing by a median of 18.8% in the acute stage (Fig. 3). Statistical analysis revealed significant differences between values measured before and immediately after CAS on both sides. In contrast, the % CBF_{az} on the ipsilateral side displayed gradual improvement, although this change was not significant. On the contralateral side, the % CBF_{az} decreased in the immediate postoperative period compared to pre-CAS levels and then returned to the pre-CAS level by 3–4 months (Fig. 4). Relative to the preoperative state, the CBV was slightly higher immediately after CAS and slightly lower at 3–4 months postoperatively (Fig. 5). The CPP increased rapidly during the acute stage and was found to have decreased on both sides at 3–4 months (Fig. 6); statistical analysis revealed significant differences between the values measured before and just after CAS on both sides.

Oxygen Extraction Fraction and $CMRO_2$

The OEF on the ipsilateral side decreased slightly during the acute stage and then normalized by the 3- to 4-month assessment. Contralateral OEF increased in the acute stage after CAS and remained elevated in the long term, although the changes were minimal (Fig. 7). The ip-

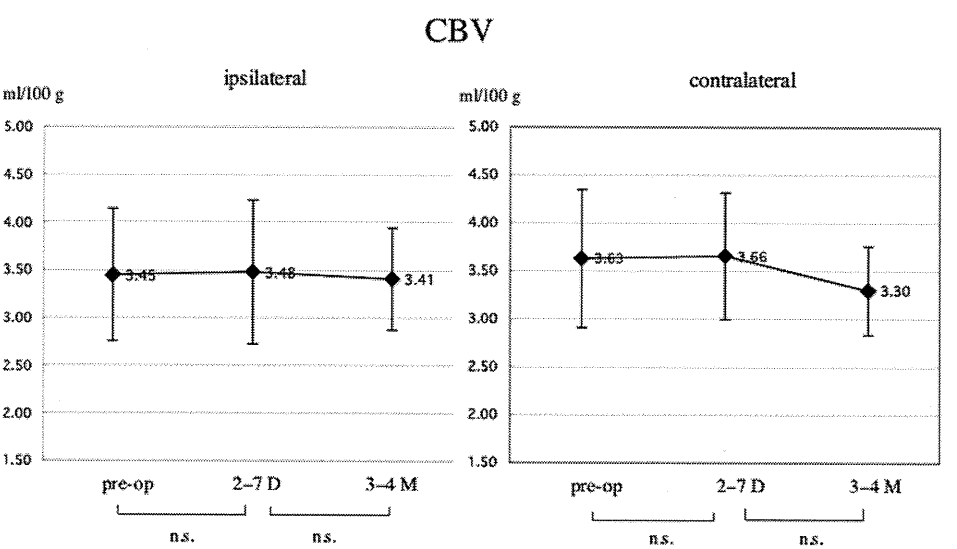

FIG. 5. Graphs showing sequential changes in CBV. Ipsilateral mean values were slightly higher in the acute stage than preoperatively, but decreased in the chronic stage.

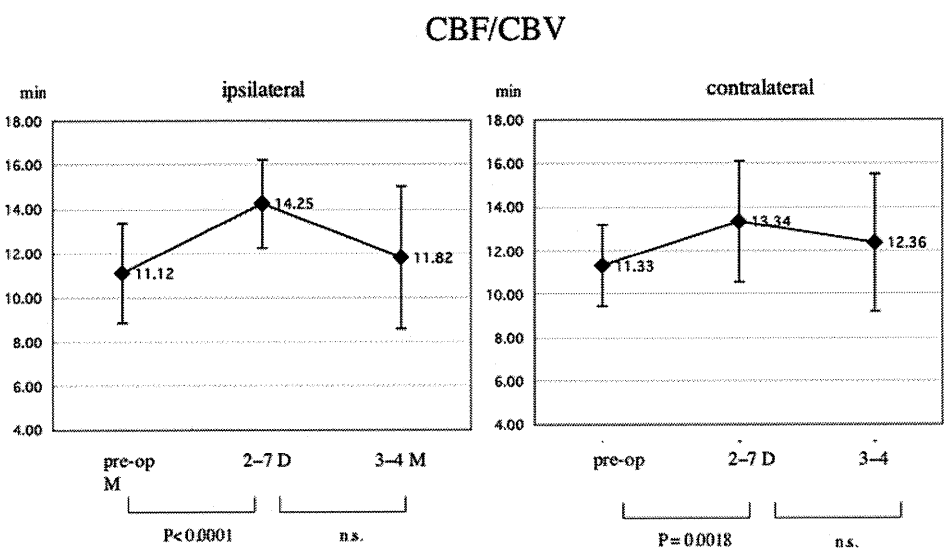

FIG. 6. Graphs showing sequential changes in CPP. Both the ipsilateral and contralateral mean CPP increased significantly in the acute stage but increased only modestly in the chronic stage.

silateral $CMRO_2$ increased slightly immediately after CAS and remained elevated at the 3- to 4-month visit, although this increase was not statistically significant (Fig. 8).

The ratio of ipsilateral to contralateral values (asymmetry index) for CBF_{rest}, % CBF_{az}, CBV, OEF, and $CMRO_2$ tended to approach 1.0 over time (Fig. 9). We noted that % CBF_{az} displayed gradual improvement, whereas CBF_{rest} increased rapidly in the postoperative acute stage before returning to normal levels by 3–4 months postoperatively. In contrast, the OEF temporarily decreased in the acute stage before normalizing over the long term. Ipsilateral values of CBF_{rest} and $CMRO_2$ exceeded contralateral values in the acute stage.

Discussion

Improvements in Cerebral Circulation

The CBF_{rest} was slightly higher at 3–4 months after CAS than it had been preoperatively. In particular, a significant increase in CBF_{rest} of ~ 30% was observed during the acute stage, demonstrating that CAS improves cerebral circulation. This rapid increase in blood flow during the acute stage diminished over time due to arteriolar self-regulation to maintain constant cerebral perfusion and resistance. The CBF at 3–4 months postoperatively was stable and slightly higher than preoperative values. The same trend was seen on the contralateral side, where an increase of 18.8% was seen in the acute stage compared to preoperative values. This increase is thought to reflect blood flow from the collateral circulation via the anterior communicating artery or leptomeningeal anastomosis. Contralaterally, increased CBF immediately after surgery has previously been confirmed by SPECT studies after CEA.[15]

Vascular Reserve

In terms of % CBF_{az}, no significant difference existed

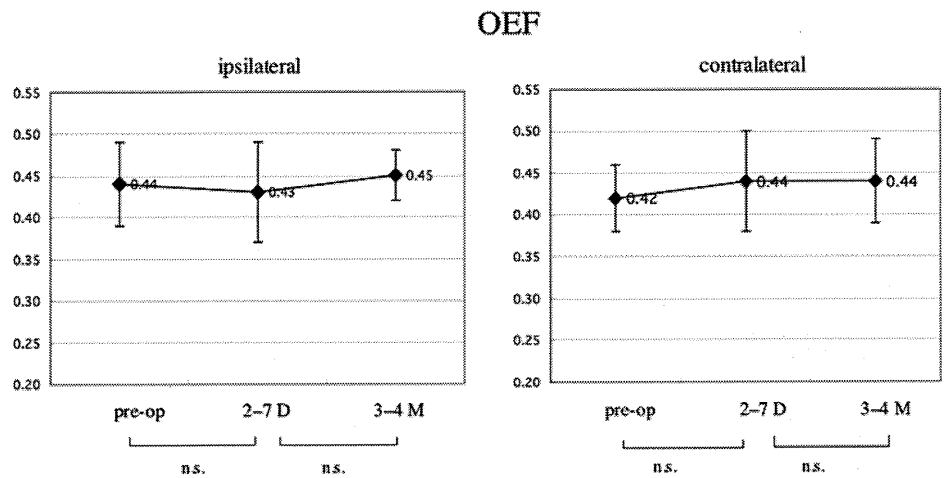

FIG. 7. Graphs showing sequential changes in OEF. The mean OEF did not significantly change at each stage.

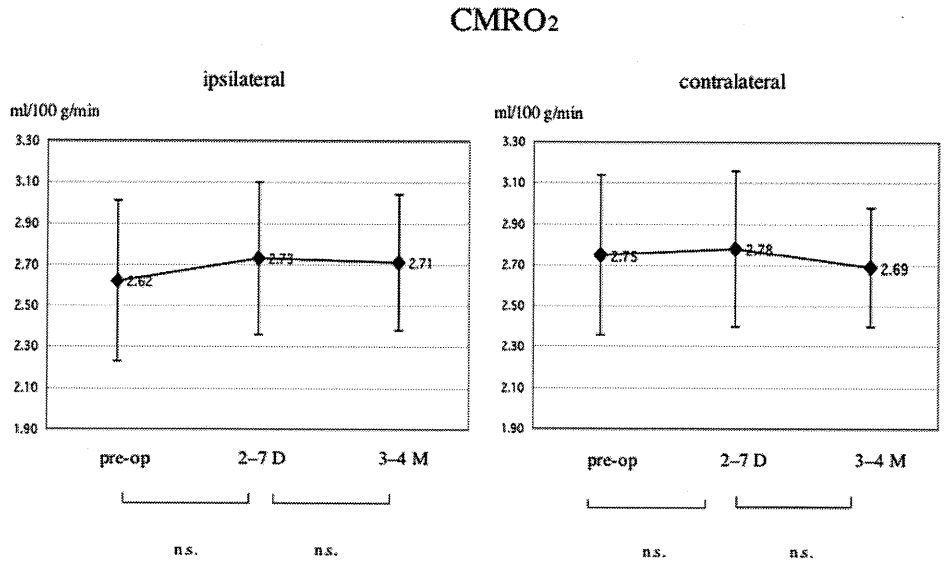

FIG. 8. Graphs showing sequential changes in $CMRO_2$. A tendency toward small increases in ipsilateral $CMRO_2$ was seen in both acute and chronic stages, although no significance differences were noted.

because of marked variations, but some improvements were seen ipsilaterally. Ours is the first study to use PET to demonstrate that stenting improves vascular reactions. On the ipsilateral site, the % CBF_{az} varied preoperatively (39.9 ± 21.5%) but increased with concomitant reductions in variation to 42.8 ± 17.4% in the acute, and 53.6 ± 13.0% at 3–4 months postoperatively. This improvement was marked, showing the greatest degree of improvement compared to the other parameters. In the present study, preoperative cerebrovascular reactivity to acetazolomide in many patients was relatively well maintained at an average of 39.9%; this suggests that marked improvement can be expected in patients with misery perfusion.

Cerebral Blood Volume

Cerebral blood volume is closely related to arteriolar dilation, and increases if vascular stenosis causes decreases in perfusion pressure. Recently Martin et al.[23] performed perfusion MR imaging before and immediately after CAS to assess changes in cerebral circulation; they reported that although there was a small bilateral increase in regional CBV (6%) after stent placement, this was much smaller than the variability observed between 2 different measurements (20%). Wilkinson and associates[35] also documented no significant differences or changes in regional CBV evaluated on perfusion MR imaging between hemispheres before and within 3 hours of

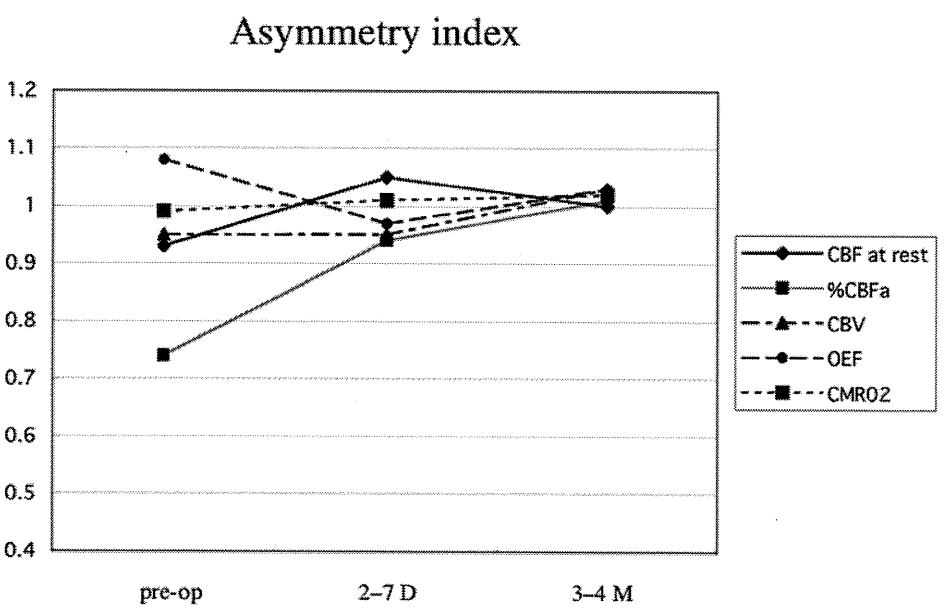

FIG. 9. Graph of asymmetry index. Indices for all parameters approached 1.0 over time. Note that the index for % CBF_{az} increased with time, while the index for CBF_{rest} temporarily exceeded 1.0 in the postoperative acute stage.

CAS. In the present study, CBV increased slightly immediately after surgery and was slightly lower at 3–4 months than it had been preoperatively; this finding did not reach statistical significance. During the acute stage the CBV did not decrease even though the perfusion pressure increased; this finding might be attributable to the arterioles not contracting immediately after surgery. Although Hosoda et al.[15] did not measure CBV, based on SPECT data obtained before and after CEA, these authors noted that abrupt restoration of CPP immediately after surgical correction of a tight ICA stenosis cannot be compensated for by vasoconstriction. However the arterioles presumably contracted to normal size over the long term, thus lowering the CBV.

Cerebral Metabolism

On the ipsilateral side, $CMRO_2$ increased after CAS, albeit insignificantly. This tendency was especially pronounced in the acute stage. Hence, rapid reperfusion to a cerebrum that has been in a state of chronic ischemia may act via some mechanism to increase oxygen metabolism. Marchal and colleagues[21,22] used PET scanning to analyze the hyperperfused regions in 10 patients with cerebral infarctions. Compared to the healthy side, CBF and CBV increased, OEF decreased, and $CMRO_2$ increased moderately. This postischemic oxygen hypermetabolism could involve the following mechanisms: 1) overexcitation of cellular metabolism (such as specific protein synthesis, oxidative phosphorylation, adenosine triphophate formation, synthesis of transcription factors, or growth factors) in cells destined to survive; or 2) excessive firing of neurons undergoing irreversible damage from a massive release of excitatory amino acids during the period of ischemia or early noxious inflammatory processes.[30,32] Consistent with this hypothesis, Heiss et al.[11] used PET in 5 patients with acute stroke, reported an increased ^{11}C-aminoacid (L-methionine) uptake in penumbral tissue surrounding the infarction and experiencing reversible ischemia. In the patients in the present study, stenting was performed for various degrees of cerebral ischemia to restore CBF; hyperemia (hyperperfusion) existed to varying degrees in the acute stage. The changes we observed in the 4 parameters (CBF, CBV, OEF, and $CMRO_2$) before and immediately after CAS matched Marchal and colleagues' findings. Based on our PET results, the state immediately after CAS could resemble hyperperfusion. However Marchal et al. described a hypermetabolic state in the ischemic region of the brain while we identified a hyperperfusion-like phenomenon in a nonischemic region of a brain with asymptomatic CA stenosis, so the parallel may not be exact. We assume, however, that patients with restlessness or headaches after CAS may not only have an increased CBF, but a significantly increased $CMRO_2$. Accumulated data are needed to investigate this issue further.

We saw no significant changes in OEF in our patients, but different results might be obtained in patients with misery perfusion. Unlike in ICA occlusion, the number of misery perfusion cases in which the OEF is ≥ 0.53 should be low in ICA stenosis. Cerebral circulation is assessed on SPECT in patients with misery perfusion because CAS is generally performed soon after onset. As mentioned above, if hyperperfusion occurs immediately after surgery, the OEF should theoretically decrease in response to increased blood flow.

Cerebral Perfusion Pressure

Cerebral perfusion pressure (CBF/CBV) rapidly increased during the acute stage. This rapid increase probably indicated that the vasoparalyzed cerebral vessels were unable to react quickly to reperfusion and thus took in much more blood at a low vascular resistance. Over time, self-regulation works to increase vascular resistance and lower CPP; however, vascular reconstruction after surgery increases CPP. The same phenomenon was seen on the healthy side.[14] Recent perfusion MR imaging studies have also found a decrease in transit time in the treated hemisphere after stent placement. Because an inverse relationship exists between transit time and perfusion pressure, our results support these earlier results.[23,35]

Cerebral perfusion pressure is generally considered to reflect cerebral vascular reserve, but our results demonstrate that this is not necessarily the case. The mean % CBF_{az} increased progressively on the ipsilateral side (Fig. 4), but was slightly higher 3–4 months postoperatively than before CAS. The mean % CBF_{az} showed a transient increase in the acute stage (Fig. 6). The reason for unmatched changes in CPP and % CBF_{az} is that although the CPP improved rapidly soon after CAS and then settled afterwards, vascular reserve improved more gradually. In other words, within 1 week of CAS, arterioles that were dilated preoperatively began to contract. Positron emission tomography captured this imbalance at a stage when more CBF was present than necessary—the preparatory stage for hyperperfusion. In hyperperfusion, the close relationship between perfusion pressure and vasodilation reserve breaks down. Over the long-term, however, these parameters are dependent on each other and are higher than in the preoperative period. Changes in CPP and vascular reserve over time after vascular reconstruction therefore differ.

Hyperperfusion syndrome has been reported after CEA and CAS. Patients with hyperperfusion syndrome can experience headaches or convulsions 2–7 days after surgery and sometimes suffer cerebral hemorrhage.[1,7,10,25,29,31] Decreased vascular reserve on preoperative SPECT images has been reported as a predictor of this syndrome.[15,17,27] We found that CPP significantly increased within 1 week of surgery, and that cerebral arterioles could not maintain normal perfusion because of this rapid increase in perfusion pressure. If the vascular walls of arterioles are damaged and permeability is increased, cerebral edema and convulsions can occur. Postoperative infarction or anticoagulant administration also risks cerebral hemorrhage.[12] These findings suggest that the acute stage after CAS is the most dangerous because CPP is abnormally high and vasodilation persists at the arteriolar level. Analysis of preoperative CBV measurements assessed with perfusion MR imaging may help to identify patients at risk for cerebral hyperperfusion after CEA.[6]

In the present study, no patient met the criteria for

postoperative hyperperfusion defined as a CBF increase of ≥ 100%; no laterality of preoperative CPP was present. We believe, however, that a marked decrease in preoperative CPP is a potential risk factor for cerebral hyperperfusion because the value of CPP is strongly associated with the value of CBV.

Study Limitations

Carotid artery stenting is indicated for ICA stenosis > 70%. Because CAS is mainly performed to prevent artery-to-artery embolism, the number of patients with severely decreased CBF was low in the present study. Only 1 patient with misery perfusion displayed an OEF ≥ 0.52, while the rate of CBF_{az} was ≤ 10% in only 2 patients (reduced vascular reserve). From the perspective of cerebral circulation and metabolism, little change was seen in OEF or $CMRO_2$ because there were few patients with severely decreased CBF and metabolism preoperatively. Furthermore, there were only 16 patients included in the study, and 3- to 4-month follow-up data were obtained in only 8 patients.

Conclusions

Repeated PET studies confirmed improvements in CBF, CPP, and oxygen metabolism after CAS. In particular, vascular reserve tended to improve gradually over time, whereas CBF, CPP, and $CMRO_2$ increased rapidly and peaked in the acute stage. Our PET study results support the hypothesis that a large discrepancy between rapidly increased CBF, CPP, and small increases in vascular reserve in the acute stage could cause hyperperfusion syndrome after CAS.

Disclaimer

The authors report no conflict of interest concerning the materials or methods used in this study or the findings specified in this paper.

Acknowledgments

The authors thank Drs. Eku Shimosegawa, Hiroshi Ito, Kumiko Okane, Atsushi Umetsu, Keiichi Ishigame, Ken Okada, and Hatsune Hirota and other staff for their assistance with PET. The authors also thank Hiromi Nishimura for his efforts in computer analysis of the PET data.

Reference

1. Abou-Chebl A, Yadav JS, Reginelli JP, Bajzer C, Bhatt D, Krieger DW, et al: Intracranial hemorrhage and hyperperfusion syndrome following carotid artery stenting: risk factors, prevention, and treatment. **J Am Coll Cardiol 43:**1596–1601, 2004
2. Cikrit DF, Dalsing MC, Harting PS, Burt RW, Lalka SG, Sawchuk AP, et al: Cerebral vascular reactivity assessed with acetazolamide single photon emission computer tomography scans before and after carotid endarterectomy. **Am J Surg 174:**193–197, 1997
3. Derdeyn CP, Cross DT III, Moran CJ, Dacey RG Jr: Reversal of focal misery perfusion after intracranial angioplasty: case report. **Neurosurgery 48:**436–439, 2001
4. Executive Committee for the Asymptomatic Carotid Atherosclerosis Study: endarterectomy for asymptomatic carotid stenosis. **JAMA 273:**1421–1428, 1995
5. Fessler RD, Lanzino G, Guterman LR, Miletich RS, Lopes DK, Hopkins LN, et al: Improved cerebral perfusion after stenting of a petrous carotid stenosis: technical case report. **Neurosurgery 45:**638–642, 1999
6. Fukuda T, Ogasawara K, Kobayashi M, Komoribayashi N, Endo H, Inoue T, et al: Prediction of cerebral hyperperfusion after carotid endarterectomy using cerebral blood volume measured by perfusion-weighted MR imaging compared with single-photon emission CT. **AJNR Am J Neuroradiol 28:**737–742, 2007
7. Friedman JA, Kallmes DF, Wijdicks EF: Thalamic hemorrhage following carotid angioplasty and stenting. **Neuroradiology 46:**399–403, 2004
8. Gibbs JM, Wise RJ, Leenders KL, Jones T: Evaluation of cerebral perfusion reserve in patients with carotid-artery occlusion. **Lancet 1:**310–314, 1984
9. Guimaraens L, Sola MT, Matali A, Arbelaez A, Delgado M, Soler L, et al: Carotid angioplasty with cerebral protection and stenting: report of 164 patients (194 carotid percutaneous transluminal angioplasties). **Cerebrovasc Dis 13:**114–119, 2002
10. Hartmann M, Weber R, Zoubaa S, Schranz C, Knauth M: Fatal subarachnoid hemorrhage after carotid stenting. **J Neuroradiol 31:**63–66, 2004
11. Heiss WD, Herholz K, Jacobs A, Duncan D, Bauer B, Huber M, et al: Increased amino-acid uptake in acute reversible focal ischemia. **J Cereb Blood Flow Metab 13 (1 Suppl):**S564, 1993 (Abstract)
12. Henderson RD, Phan TG, Piepgras DG, Wijdicks EF: Mechanisms of intracerebral hemorrhage after carotid endarterectomy. **J Neurosurg 95:**964–969, 2001
13. Henry M, Henry I, Klonaris C, Masson I, Hugel M, Tzvetanov K, et al: Benefits of cerebral protection during carotid stenting with the PercuSurge GuardWire system: midterm results. **J Endovasc Ther 9:**1–13, 2002
14. Hino A, Tenjin H, Horikawa Y, Fujimoto M, Imahori Y: Hemodynamic and metabolic changes after carotid endarterectomy in patients with high-degree carotid artery stenosis. **J Stroke Cerebrovasc Dis 14:**234–238, 2005
15. Hosoda K, Kawaguchi T, Shibata Y, Kamei M, Kidoguchi K, Koyama J, et al: Cerebral vasoreactivity and internal carotid artery flow help to identify patients at risk for hyperperfusion after carotid endarterectomy. **Stroke 32:**1567–1573, 2001
16. Hosoda K, Fujita S, Kawaguchi T, Shose Y, Shibata Y, Tamaki N, et al: Influence of degree of carotid artery stenosis and collateral pathways and effect of carotid endarterectomy on cerebral vasoreactivity. **Neurosurgery 42:**988–994, 1998
17. Kaku Y, Yoshimura S, Kokuzawa J: Factors predictive of cerebral hyperperfusion after carotid angioplasty and stent placement. **AJNR Am J Neuroradiol 25:**1403–1408, 2004
18. Kanno I, Iida H, Miura S, Murakami M, Takahashi K, Uemura K, et al: A system for cerebral blood flow measurement using an $H_2{}^{15}O$ autoradiographic method and positron emission tomography. **J Cereb Blood Flow Metab 7:**143–153, 1987
19. Kashiwazaki D, Kuroda S, Ushikoshi S, Shichinohe H, Ishikawa T, Asano T, et al: [Normalization of cerebral hemodynamics and metabolism after carotid stenting in patients unfit for major surgery.] **No Shinkei Geka 31:**1315–1320, 2003 (Jpn)
20. Ko NU, Achrol AS, Chopra M, Saha M, Gupta D, Smith WS, et al: Cerebral blood flow changes after endovascular treatment of cerebrovascular stenoses. **AJNR Am J Neuroradiol 26:**538–542, 2005
21. Marchal G, Furlan M, Beaudouin V, Rioux P, Hauttement JL, Serrati C, et al: Early spontaneous hyperperfusion after stroke, a marker of favourable tissue outcome? **Brain 119:**409–419, 1996
22. Marchal G, Young AR, Baron JC: Early postischemic hyper-

perfusion: pathophysiologic insights from positron emission tomography. **J Cereb Blood Flow Metab 19:**467–482, 1999
23. Martin AJ, Saloner DA, Roberts TP, Roberts H, Weber OM, Dillon W, et al: Carotid stent delivery in an XMR suite: immediate assessment of the physiologic impact of extracranial revascularization. **AJNR Am J Neuroradiol 26:**531–537, 2005
24. Mas JL, Chatellier G, Bevssen B, Branchereau A, Moulin T, Becquemin JP, et al: Endarterectomy versus stenting in patients with symptomatic severe carotid stenosis. **N Engl J Med 355:**1660–1671, 2006
25. McCabe DJH, Brown MM, Clifton A: Fatal cerebral reperfusion hemorrhage after carotid stenting. **Stroke 30:**2483–2486, 1999
26. North American Symptomatic Carotid Endarterectomy Trial Collaborators: Beneficial effect of carotid endarterectomy in symptomatic patients with high grade carotid stenosis. **N Engl J Med 325:**445–453, 1991
27. Ogasawara K, Yukawa H, Kobayashi M, Mikami C, Konno H, Terasaki K, et al: Prediction and monitoring of cerebral hyperperfusion after carotid endarterectomy by using single-photon emission computerized tomography scanning. **J Neurosurg 99:**504–510, 2003
28. Ohki T, Veith FJ, Grenell S, Lipsitz EC, Gargiulo N, McKay J, et al: Initial experience with cerebral protection devices to prevent embolization during carotid artery stenting. **J Vasc Surg 36:**1175–1185, 2002
29. Penn AA, Schomer DF, Steinberg GK: Imaging studies of cerebral hyperperfusion after carotid endarterectomy, case report. **J Neurosurg 83:**133–137, 1995
30. Pulsinelli W: Pathophysiology of acute ischaemic stroke. **Lancet 339:**533–536, 1992
31. Shinno K, Ueda S, Uno M, Nishitani K, Nagahiro S, Harada M: [Hyperperfusion syndrome following carotid endarterectomy: evaluation using diffusion-weighted magnetic resonance imaging: case report.] **Neurol Med Chir (Tokyo) 38:**557–561, 1998 (Jpn)
32. Stoll G, Jander S, Schroeter M: Inflammation and glial responses in ischemic brain lesions. **Prog Neurobiol 56:**149–171, 1998
33. Uchiyama N, Kida S, Watanabe T, Yamashita J, Matsui O: Improved cerebral perfusion and metabolism after stenting for basilar artery stenosis: technical case report. **Neurosurgery 48:**1386–1392, 2001
34. Uno M, Harada M, Nagahiro S: Quantitative evaluation of cerebral metabolites and cerebral blood flow in patients with carotid stenosis. **Neurol Res 23:**573–580, 2001
35. Wilkinson ID, Griffiths PD, Hoggard N, Cleveland TJ, Gaines PA, Macdonald S, et al: Short-term changes in cerebral microhemodynamics after carotid stenting. **AJNR Am J Neuroradiol 24:**1501–1507, 2003
36. Yadav JS, Wholey MH, Kuntz RE, Fayad P, Katzen BT, Mishkel GJ, et al: Protected carotid-artery stenting versus endarterectomy in high-risk patients. **N Engl J Med 351:**1493–1501, 2004

Manuscript submitted March 15, 2007.
Accepted September 19, 2008.
Please include this information when citing this paper: published online March 20, 2009; DOI: 10.3171/2008.9.17663.
Address correspondence to: Akifumi Suzuki, M.D., Ph.D., 6-10, Senshu-Kubota-machi, Akita 010-0874, Japan. email: akifumi@akita-noken.go.jp.